Dynamical wavelength selection by tilt domains in thin-film lamellar eutectic growth

G. Faivre and J. Mergy
Groupe de Physique des Solides, Universités Paris 7 et Pierre et Marie Curie, Tour 23, 2 place Jussieu, 75251 Paris CEDEX 05, France
(Received 13 March 1992)

Tilt domains are dynamical defects of cellular growth fronts consisting of a group of asymmetric cells traveling laterally along the front. We study the dynamics of these defects in thin-film directional solidification of the CBr_4-C_2Cl_6 eutectic alloy. We show that the sweeping of the growth front by tilt domains, at a given growth velocity V, brings it into a well-defined "dynamically selected" state. Once this state is reached, the tilt domains travel with a constant width. A sudden increase (decrease) of the growth velocity transforms constant-width tilt domains to growing (shrinking) ones. This behavior is in complete agreement with the theoretical predictions made by Coullet *et al.* [Phys. Rev. Lett. **63**, 1954 (1989)] and Caroli *et al.* [J. Phys. I (Paris) **2**, 281 (1992)]. We study the V dependence of the dynamically selected wavelength. It does not follow the $V^{-1/2}$ law, contrary to the "selected" wavelength of lamellar eutectics in the range of velocities and thermal gradients that we use. Above a velocity V_{cr}, the dynamically selected basic state is unstable against the lamellar-extinction instability. We describe some dynamical patterns resulting from the interplay between the latter instabiilty and the tilt instability.

PACS number(s): 64.70.Dv, 81.10.Fq, 03.40.−t

I. INTRODUCTION

Recent observations on various types of cellular fronts have revealed the existence of a dynamical defect consisting of a group of deformed cells traveling laterally at constant velocity along the front [1–3]. These "tilt domains" (so called, in lamellar eutectics, because they give rise to lamellae tilted with respect to the growth direction; see below) erase the cellular pattern into which they are advancing and leave behind a new untilted cellular pattern. It was found that, in some cases, the wavelength of the new pattern was more uniform and had a different average value than that of the initial pattern [1]. These first observations brought Coullet *et al.* [4] to propose a phenomenological model of the dynamics of tilt domains, but the existing data were not extensive enough to allow quantitative confirmation of the predictions of this model.

In this paper, we present a detailed experimental investigation of the dynamics of tilt domains, which establishes the validity of the phenomenological model. The experimental system is the lamellar eutectic alloy CBr_4-C_2Cl_6 directionally solidified in thin films, in which we have recently observed the homogeneous tilt bifurcation [5]. In lamellar eutectics, it is a well-known result that, under certain conditions, the solidification front stabilizes into a periodic structure of rather well-defined average wavelength, the spatial dispersion of which is nevertheless not negligible [6–10]. We consider in this paper the relationship between the dynamical wavelength selection by tilt domains and this long-standing, but still unclear, "wavelength-selection problem."

The phenomenological model assumes a bifurcation between two types of stationary, periodic states of the system: the "basic" states, in which the shape of the cells is symmetric with respect to the growth direction and the tilted states, in which this symmetry is broken and the pattern is drifting laterally at constant velocity. A sketch of these patterns in the case of a lamellar eutectic system is given in Fig. 1. That such a tilt bifurcation actually exists in our system has been proven recently numerically by Kassner and Misbah [11,12] and experimentally [5]. A sketch of the tilt bifurcation diagram is shown in Fig. 2(a). The control parameter for the bifurcation is $\lambda^2 V$, where λ is the wavelength of the pattern and V the pulling velocity, in agreement with the scaling law established by Kassner and Misbah for small values of the ratio G/V, where G is the thermal gradient [14]. It must be stressed that the states represented by the continuous curves in Fig. 2(a) are not necessarily stable against other

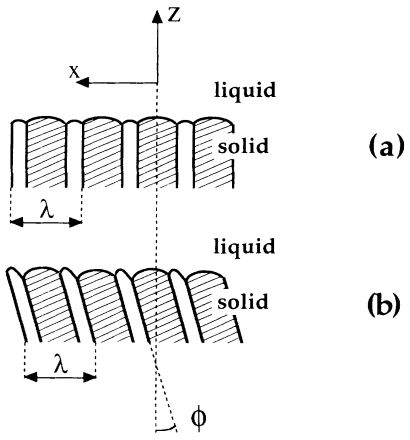

FIG. 1. Sketches of the stationary, periodic states of lamellar eutectic fronts (a) symmetric "basic" state; (b) asymmetric "tilted" state. Z, growth or "pulling" direction; X, lateral direction; λ, wavelength or "lamellar spacing"; ϕ, tilt angle (defined by $\tan\phi = V_x/V$; V, pulling velocity; V_x, drift velocity).

destabilization mechanisms (phase diffusion, oscillations, etc.) than those that depict the response of the system to the tilt instability.

The existence of space-filling tilted states naturally leads to the interpretation of tilt domains illustrated by Fig. 2 [2,15]. The tilted pattern within the domain (T) and the untilted ones ahead (A) and in the rear (R) of it are regions of space-filling, stationary states, represented by points belonging to the curves drawn in Fig. 2(a) (the exact position of these points is to be discussed later on.) The two narrow regions limiting the tilt domain are "kinks" or "walls" between space-filling states, moving laterally with stationary profiles and velocities. Although eight variables seem necessary to describe a tilt domain—the wavelengths and tilt angles of the three patterns (surface-tension anisotropy causes the basic state to be slightly tilted; see below) and the velocities of the two walls—only three of them are in fact independent:

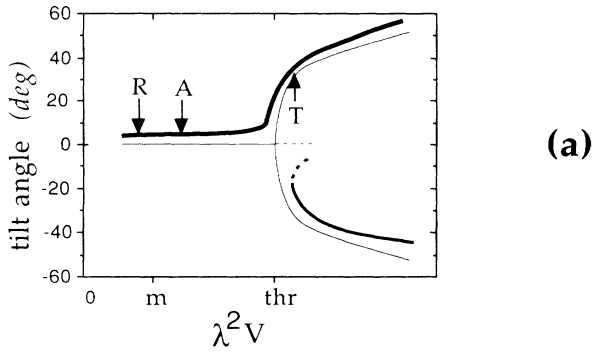

FIG. 2. (a) Sketch of the tilt bifurcation diagram for the CBr_4-C_2Cl_6 alloy, for concentrations near the middle of the eutectic plateau. ϕ, tilt angle; λ, wavelength; V, pulling velocity (see Fig. 1). The control parameter for the bifurcation is $\lambda^2 V$. On the $\lambda^2 V$ axis: m, minimum undercooling; thr, bifurcation threshold. $(\lambda^2 V)_{\rm thr}$ is about $4(\lambda^2 V)_m$. A forward pitchfork bifurcation (fine-line curves) has been found numerically by Kassner and Misbah [11,12] in a model ignoring surface-tension anisotropy. The bifurcation actually observed is made imperfect by surface-tension anisotropy (bold-line curves) [5,13]. The sketch assumes a positive anisotropy-driven tilt angle ϕ_0 of the basic states. A,T,R, states ahead of, within, in the rear of the tilt domain sketched in (b). (b) Sketch of a tilt domain. Each pair of lamellae is represented by a single cell. The direction of the wall motion is opposite that of the pattern drifting (see [16]).

first, two relationships are imposed by the continuity of the lamellae through the walls [16]; second, at a given pulling velocity, the tilt angle is a definite function of the wavelength (for a given sign of the tilt angle in the domain). Thus, according to this interpretation, any conceivable tilt domain at given V is completely specified by, for instance, the wavelengths of the three patterns ahead of, within, and in the rear of the domain. The model establishes additional relationships between these variables.

We shall now briefly describe the phenomenological model. In the initial version; the tilt bifurcation was assumed to be subcritical [4]. This seemed a necessary condition for the existence of a domain of the tilted state within the untilted one. The above-mentioned numerical and experimental results, however, showed that, in our system, the bifurcation is forward (anisotropy effects can be ignored, to the first approximation). Caroli, Caroli, and Fauve have modified the initial version of the model in order to show that tilt domains are compatible with a forward tilt bifurcation [17], as observed in our system. The breaking of the symmetry of the front shape with respect to the growth direction gives rise at the same time to the drift of the pattern along the front, i.e., to an intrinsic coupling between tilt and phase dynamics. It is the supplementary degree of freedom associated with the phase of the pattern (i.e., with the existence of infinite families of solutions above and below the bifurcation indexed by λ) that permits domains to exist even when the bifurcation at fixed λ is forward. We shall closely follow Caroli, Caroli, and Fauve's version of the model.

An asymmetry parameter A, the amplitude of the antisymmetric part of the front profile, is introduced. Two coupled equations for A and the phase Φ of the pattern are written as

$$A_t = \mu A - \alpha A^3 + A_{xx} + \epsilon A \Phi_x + \gamma A A_x \ , \tag{1a}$$

$$\Phi_t = \mathcal{D}\Phi_{xx} + \omega A \ , \tag{1b}$$

where the indices denote derivation with respect to position x along the front and time t [18]. The connection with experiments is established as follows. Equations (1) describe deviations from a homogeneous symmetric ($A=0$) state of given wavelength λ_0 (or wave vector q_0) near the tilt bifurcation threshold. The local pattern wavelength λ (or wave vector q) and drift velocity V_x are given by

$$q - q_0 = \Phi_x \tag{2a}$$

and

$$V_x = -\Phi_t / q \cong -\Phi_t / q_0 \ . \tag{2b}$$

For homogeneous states (A and Φ_x uniform), the drift velocity is $-\omega A / q_0$. The bifurcation from symmetric ($A=0$) to asymmetric ($A \neq 0$) states with wave vector q occurs for $\mu + \epsilon \Phi_x = 0$. Thus, at fixed wavelength, the control parameter for the bifurcation is μ, but the threshold value $\mu_{\rm thr}$ depends on the wavelength. Therefore, μ is to be identified with the pulling velocity, or, more precisely, with $V - V_0$, where V_0 is the velocity threshold for $\lambda = \lambda_0$ (equivalently, λ_0 is the wavelength threshold for

$V=V_0$). To reproduce the observed behavior, one has furthermore to assume that μ increases as V increase and $\epsilon<0$. The bifurcation is forward if $\alpha>0$ and the stationary states show Eckhaus stability if $\mathcal{D}>0$.

The coupling term $\epsilon A\Phi_x$ gives rise to a continuous set of stable states, indexed by their wavelengths, to exist for a given value of μ. In order to explain the existence of tilt domains, one has to show that, at a given μ, stationary walls can exist between two stable states of different wavelengths. The results can be expressed as follows.

(i) At fixed V, for a given value of the wavelength ahead of the domain λ_A [see Fig. 3(a)], the condition that the leading wall is stationary determines the values of the velocity of the wall v_A and the wavelength in the domain λ_T. Similarly, for a given value of λ_T, the condition that the trailing wall is stationary determines the values of the velocity of the wall v_R and the wavelength in the rear of the domain λ_R. Thus, at fixed V and λ_A, only one type of tilt domain can be stationary: v_A, λ_T, v_R, and λ_R are functions of λ_A and V only. It is of course supposed that the width of the domain is much larger than that of the walls (the distortion of the stationary patterns by the latter decreases exponentially with distance, with a characteristic length $\mu^{-1/2}$).

(ii) At fixed V, there exists a single value of λ_A such that $v_A=v_R$, or, equivalently, $\lambda_R=\lambda_A$ (see [16]). This situation, characterized by the fact that the stationary tilt domains travel with a constant width, can be called, by analogy, the Maxwell point between the basic and the tilted states for the velocity V. Hereafter, the values of the wall velocities, basic-state, and tilted-state wavelengths at the Maxwell point will be denoted v^*, λ^*, and λ_T^*, respectively [see Fig. 3(b)]. For a given value of V, λ^* is smaller, and λ_T^* larger, than the threshold wavelength $\lambda_{\rm thr}$ for the tilt bifurcation.

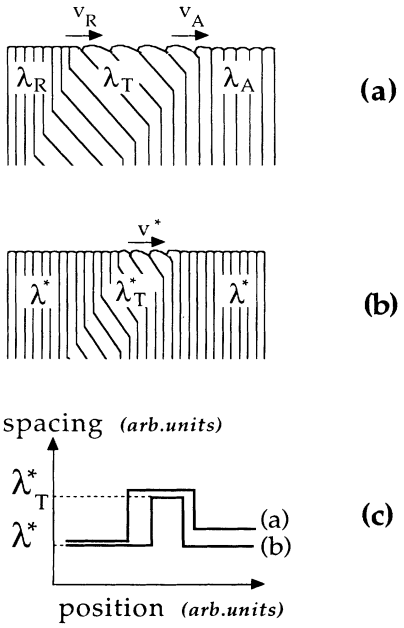

FIG. 3. Predictions the dynamical-selection model [4,17] (see the text). (a) Growing tilt domain for $\lambda_A>\lambda^*$; (b) constant-width tilt domain for $\lambda_A=\lambda^*$; (c) lamellar spacing against the position along the front, in cases (a) and (b).

(iii) At fixed V, for $\lambda_A>\lambda^*$, $v_A>v_R$, and $\lambda_R<\lambda_A$ (tilt domains are growing); for $\lambda_A<\lambda^*$, $v_A<v_R$, and $\lambda_R>\lambda_A$ (tilt domains are shrinking). In both cases, λ_R is nearer λ^* than λ_A [see Fig. 3(c)]. Thus, each domain that sweeps the front brings the system closer to the Maxwell point. This is the process called dynamical wavelength selection by tilt domains. How fast λ_R approaches λ^* cannot be predicted by the model. Hereafter, we call λ^* and λ_T^* the dynamically selected wavelengths.

(iv) Changing V is equivalent to changing the reference wave vector q_0. More precisely, $\lambda_T^*=\lambda_{\rm thr}+2K$ and $\lambda^*=\lambda_{\rm thr}-K$, where K is a positive constant depending on α, ϵ, γ, $\mathcal{D}$, and ω. By assumption, $\lambda_{\rm thr}$ decreases as V increases and so do λ^* and λ_T^*.

These predictions have, in principle, a very limited range of validity. Equations (1) are amplitude expansions near the reference values λ_0 and $V_0=V_{\rm thr}(\lambda_0)$. They retain only the first nonlinearities [19]. Thus (i) the model is only meant to describe qualitative trends in the vicinity of a reference velocity—it cannot account for the quantitative evolution of the dynamical-selection parameters over a finite range of V; (ii) the model assumes that, at given V, the local wavelength remains everywhere close to $\lambda_{\rm thr}$ and varies smoothly along the front. This condition is obviously not fulfilled in our experimental system. As previously shown [2] and confirmed below, the tilted wavelength is about twice the basic one, ϕ_T is typically 30° and the order of magnitude of the domain-wall width is only one lamellar spacing. The physical origin of this behavior of our system is probably the steepness of the tilted branch near the bifurcation threshold (for λ^2V a few percent above the critical value, ϕ is about 25°), which is itself due to the very small ratio of the capillary length to the diffusion length [12].

The phenomenological model also ignores the surface-tension anisotropies resulting from the anisotropy of the crystal phases. We have previously established that [5,10] (i) our system is composed of eutectic grains, which are regions of homogeneous crystal orientations of the two solid phases. Anisotropy effects are uniform within a given grain, and different from grain to grain; (ii) the symmetry of the basic state is, in fact, broken by capillary anisotropy: there exists a nonzero, anisotropy-driven tilt angle ϕ_0 in the basic state, the sign and magnitude of which are grain dependent; (iii) in the so-called floating grains (the only ones that we shall consider hereafter), capillary anisotropy can be considered as a weak perturbation of the system without anisotropy. Experimentally, $|\phi_0|$ is small ($<5°$); and (iv) capillary anisotropy makes the bifurcation slightly imperfect. This is illustrated by Fig. 2(a), in the case $\phi_0>0$.

These facts have two straightforward consequences as regards tilt domains. First, the quantitative characteristics of tilt domains are different in different grains (that λ_T^* is weakly grain dependent is proven by Fig. 9 of Ref. [6]). Second, in a given grain, tilt domains of tilt angles with opposite signs (hence moving in opposite directions)

do not have the same absolute values of their dynamical parameters (they are not mirror images of each other). In a given grain, we must, in principle, distinguish the domains in which ϕ_T has the same sign as ϕ_0 (primary domains) from those in which ϕ_T and ϕ_0 have opposite signs (secondary domains). In floating grains, the differences between the characteristics of tilt domains moving in opposite directions are not larger than the differences between primary domains belonging to different grains [20].

A necessary condition for the quantitative study of tilt domains is the presence in the sample of large, floating eutectic grains. The experimental scatter is mostly due to the λ gradients generated near the grain boundaries [10]. Our quantitative results (especially in Figs. 6 and 8) were obtained in grains containing more than 200 lamellar pairs. Eutectic grain boundaries also come into play as sites of "heterogeneous nucleation" of tilt domains. At the alloy concentration at which we are working and for sufficiently high pulling velocities, a slanting grain boundary emits tilt domains in a quasiperiodical way [2]. Tilt domains can also nucleate "homogeneously," i.e., far from any heterogeneity of the system, by a very interesting, but complicated, process, in which another type of instability of the basic state, the so-called oscillation at twice the basic wavelength, is involved [5,21] [see Fig. 9(b)]. This process will not be studied in this paper.

The paper is organized as follows.

(i) We describe experiments which allow a direct comparison of the tilt-domain dynamics actually observed with the qualitative predictions of the phenomenological model. The agreement is excellent, demonstrating that the model indeed captures the essential physical features of tilt domains.

(ii) We study the quantitative variation of the dynamically selected wavelengths λ^* and λ_T^* with the pulling velocity. λ_T^* is close to λ_{thr} and thus varies as $V^{-1/2}$, whereas λ^* decreases much more rapidly than $V^{-1/2}$ as V increases.

(iii) The smallest wavelength for which the basic state is stable against the lamellar-extinction or pinching-off [6] instability (λ_{pinch}) is known to vary approximately as $V^{-1/2}$, in the range of values of G/V considered here. For V larger than a value V_{cr}, λ^* is smaller than λ_{pinch}. The dynamically selected basic state (i.e., the basic state of wavelength λ^*) is then unstable to lamellar extinctions. We briefly describe various dynamical structures resulting from this instability.

II. DESCRIPTION OF THE EXPERIMENTS

The choice of the particular conditions under which the experiments were performed has been explained previously [5]. The samples are about 6 mm wide and 15 μm thick. Unless otherwise mentioned, the thermal gradient is $G \cong 80$ K cm^{-1} and the alloy concentration C is near the middle of the eutectic plateau (the volume fraction of the α phase in the solid is $\eta \cong 0.5$). Since the eutectic point of CBr_4-C_4Cl_6 is located at $\eta \cong 0.7$, the alloy in our samples is hypereutectic.

A series of experiments was performed that all gave similar results. Let us describe in detail one of these experiments. The sample is placed in the temperature gradient, in a position where the film is almost completely liquid. Since the alloy is hypereutectic, the equilibrium solid-liquid interface at rest is a single-phase β front. The presence of grain boundaries in the β phase is manifested by cusps on the otherwise perfectly planar front. After about 1 h at rest, the pulling is switched on, at velocity 1.54 μm s^{-1}. Dendrites immediately form on the β-liquid growth front, the stems of which indicate the crystal orientation of the grains [10]. A few minutes later, the dendritic front is invaded by the eutectic structure, in a way which conserves the initial grain structure. During the invasion, tilt domains nucleate at the tips of some dendrites. Thus, a few minutes after the onset, the system is already in the type of situation that we wish to study, with basic-state regions alternating with tilt domains (Fig. 4). The experiment then consists in a series of steps at constant pulling velocity separated by upward or downward velocity jumps (Table I). The same eutectic grain structure is conserved through all the velocity jumps. We thus know, at any time, to which grain a given part of the growth front belongs.

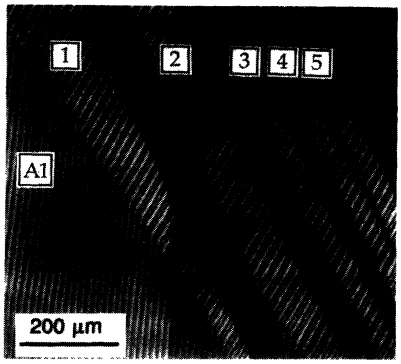

FIG. 4. Tilt domains emitted at the onset of the experiment described in Table I. $V = 1.54$ μm s^{-1}. Photograph of the solid (the solidification front is out of the image). Time is running upwards. The domains are primary ones. Note the decrease of the basic-state tilt angle when the wavelength decreases. The white dots in the upper half of the photograph are traces left by lamellar extinctions (see text).

III. RESULTS

A. Evidence for the dynamical wavelength selection

Figure 4 shows a series of five tilt domains emitted at the very beginning of the experiment described by Table I. The region shown corresponds to a single eutectic grain. The domains have just nucleated at dendrite tips

TABLE I. Successive steps at constant pulling velocity in the experiment described in the text. V, pulling velocity; Δt, duration of the step.

V (μm s^{-1})	1.54	2.26	1.54	1.22	0.85	2.26
Δt (s)	3400	3000	2900	2900	1300	2000

and are advancing into the basic-state structure resulting from the invasion process (state $A1$). Clearly, the first domain of the series (domain 1) is growing and the wavelength at its rear, λ_{R1}, is smaller than λ_{A1}. Let us, for the moment, ignore some lamellar extinctions occurring in the basic state behind the domains (we shall return to them later on). Then it is clear that the widths of the next domains (domains 2 to 5), contrary to that of the first one, remain essentially constant. This is in agreement with the predictions of the phenomenological model, provided that we admit that λ_{R1} is almost equal to λ^*. In other words, this observation indicates that the sweeping by a single domain suffices to bring the system very close to its Maxwell point for the given velocity.

Another qualitative piece of evidence for the existence of dynamical wavelength selection can be obtained by means of velocity jumps. Assume that, before the jump, the system has been pulled for a long time at velocity V_1 and contains tilt domains traveling with a constant width. This implies, in particular, that the wavelength ahead of the domains is $\lambda_1^* = \lambda^*(V_1)$. When the velocity jump is performed, the wavelength is conserved (no lamellae are created or destroyed as a result of the jump [5]). The wavelength ahead of the domain is still λ_1^*. According to the model, the dynamically selected wavelength λ^* is a decreasing function of V. If, for instance, $V_2 > V_1$ (upward jump), $\lambda_1^* > \lambda_2^* = \lambda^*(V_2)$ and the domain should grow. Similarly, it should shrink after a downward jump. This is indeed what we observed, as illustrated by Fig. 5.

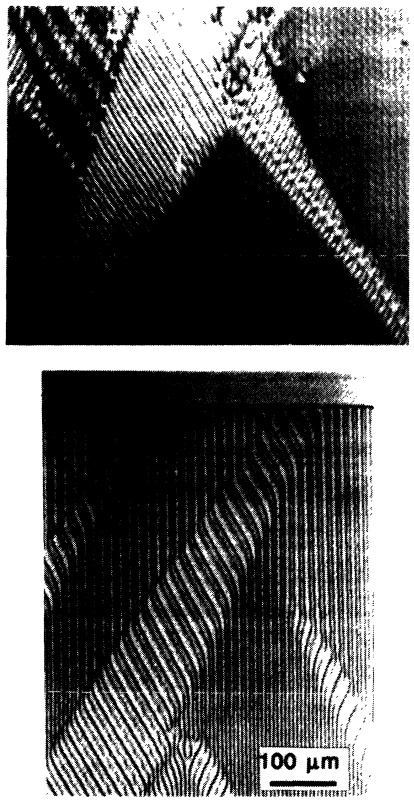

FIG. 5. Effect of velocity jumps on preexisting tilt domains. (a) Jump from 1.54 to 2.26 $\mu m\,s^{-1}$; (b) jump from 1.22 to 0.85 $\mu m\,s^{-1}$. Broken lines, velocity jump.

Observations similar to those shown in Figs. 4 and 5 have been repeated many times, at various pulling velocities, with qualitatively similar results. The wavelengths and tilt angles of the patterns and the velocities of the walls have been measured. The reproducibility is satisfactory (see below), demonstrating that λ^*, λ_T^*, etc., are well-defined, physical quantities. We therefore conclude that the agreement between the qualitative predictions of the model and the observations is complete.

Let us now turn to the quantitative analysis of the experiments. We first consider some of the above-mentioned characteristics of tilt domains, which do not depend on the pulling velocity.

(i) At constant V, according to the model, v_A, λ_T, v_R, and λ_R are functions of λ_A. We have seen that λ_R is close to λ^*, whatever λ_A. In fact, only v_A is observed to change noticeably when λ_A changes. In general, the variations of λ_T, v_R, and λ_R are not larger than the experimental uncertainty. When λ_A is not uniform, this feature manifests itself by a wavy trajectory of the leading wall, contrasting with the rectilinear trajectory of the trailing wall (this was mentioned, but not explained, in Ref. [2]). Examples of the rapid response of v_A to the variations of λ_A at constant V are clearly visible in Figs. 4 and 10 (a detailed analysis of the latter is given below).

(ii) It is difficult to obtain reliable measurements of the very small width of the domain walls. Direct measurements generally give values smaller than, say, λ_T^*. We have also analyzed the final collapse of the domains after a downward velocity jump [Fig. 5(b)]. The tilt angle within the domain is observed to decrease when the width of the domain becomes smaller than a value which we identify as the interaction distance between walls. This distance is about λ_T^*.

B. V dependence of λ^* and λ_T^*

Figure 6(a) shows a plot of the lamellar spacing against the position of the lamellar pair along the growth front at a given time [$\lambda(x)$ plot], taken during the course of a process analogous to that shown in Fig. 4. The region scanned belonged to a single, very large eutectic grain. The seven tilt domains visible on the scan have been emitted near the right-hand-side grain boundary and were traveling to the left at the time of the scan. The average values of the lamellar spacings within the successive basic-state regions and tilt domains are given in Fig. 6(b). The instrumental error is ± 1 μm on the domain width and $\pm 1/n$ μm on the average wavelength, where n is the number of lamellar pairs in the domain. The bars in the figure represent the experimental width of the λ distribution within the domains. Figure 6 shows that, under favorable circumstances, the experimental uncertainty on λ^* and λ_T^* is about ± 1 μm. With this accuracy, it can be seen, for instance, that sweeping by more than one domain is in fact necessary for λ^* to be reached, although most of the wavelength readjustment is performed by the first domain (see also Fig. 10 below.)

Figure 7 gives, as functions of V, the values of λ^*, λ_T^*,

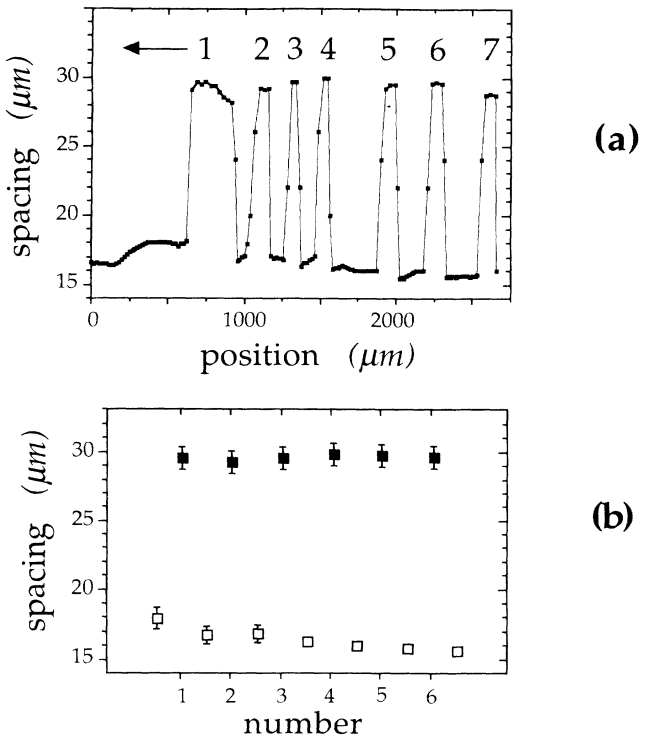

FIG. 6. (a) Lamellar spacing against the position along the front. $V=0.85\ \mu m\,s^{-1}$, $G\cong 33\ K\,cm^{-1}$, and $\eta\cong 0.47$. The region shown is included in a single eutectic grain. The tilt domains are traveling to the left (arrow); (b) average lamellar spacings within the tilt domains, numbered as in (a) (full symbols) and in the basic-state regions between the domains (open symbols).

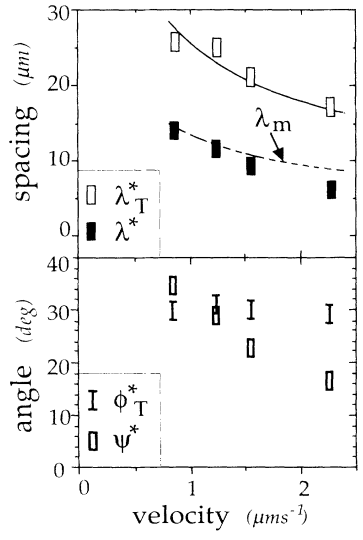

FIG. 7. Dynamically selected characteristics as functions of the pulling velocity (see text for symbols). Measurements performed in the primary tilt domains of a given eutectic grain during the experiment described in Table I. Continuous curve, numerical fit assuming $\lambda_T^*\sim V^{-1/2}$. Broken curve, estimated value of the minimum-undercooling wavelength.

ϕ_T^*, and $\psi^*=\tan^{-1}(v^*/V)$ for the primary domains of a given grain, during the experiment described in Table I. The same measurements are represented in a logarithmic plot in Fig. 8(a). A numerical fit of the data by a power law shows that, as V increases, λ_T^* varies as $V^{-1/2}$, within experimental uncertainty, while λ^* decreases more rapidly than $V^{-1/2}$. That λ^* and λ_T^* do not have the same V dependence is confirmed by the decrease of ψ^* as V increases. The fact that ϕ_T^* does not depend on V while λ_T^* varies as $V^{-1/2}$ indicates that the tilted pattern within the domain obeys the same scaling laws as the spacing-filling homogeneous states, which supports the assumption that it is a portion of one of these states. More precisely, we find, for the results of Fig. 8, $(\lambda_T^*)^2V=680\pm70\ \mu m^3\,s^{-1}$. [In Fig. 6, for a slightly different alloy concentration, we find $(\lambda_T^*)^2V=740\pm50\ \mu m^3\,s^{-1}$.] The value that we have previously found for the tilt bifurcation threshold is $\lambda_{thr}=680\pm40\ \mu m^3\,s^{-1}$ [5]. This result is satisfactory. Because of the steepness of the bifurcation, the value of λ^2V needs to be only a few percent above the threshold value for the tilt angle within the domain to be about 30°. In other words, it is ϕ_T^* which really measures the distance of the dynamically selected tilted state from the bifurcation threshold. We find that this distance is constant, within experimental uncertainty, over the velocity range explored.

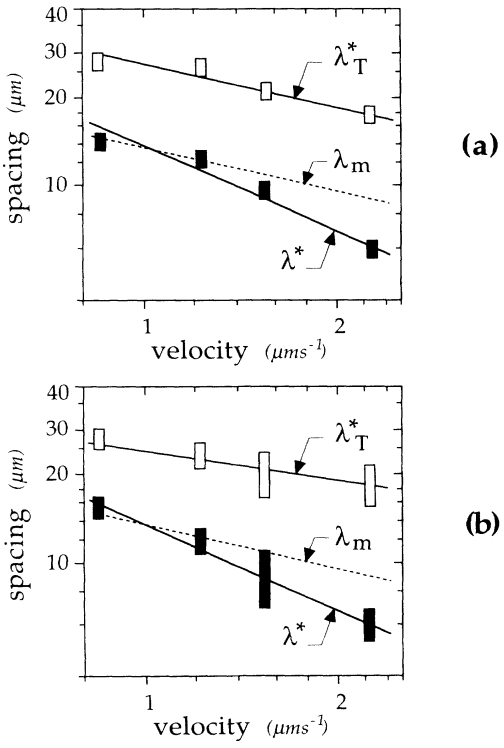

FIG. 8. Dynamically selected characteristics as functions of the pulling velocity; (a) same measurements as in Fig. 7; (b) measurements performed in a number of different grains. Continuous curves, numerical fit by power laws (best-fit exponents: for λ_T^*, 0.45 ± 0.5; for λ^*, 0.95 ± 0.5). Broken curve, as in Fig. 7.

These conclusions are not grain dependent. Figure 8(b) represents data obtained in various samples, and therefore in various eutectic grains. Numerical fittings on these sets of values give the same results as in Fig. 8(a). The dispersion of the measured values primarily reflects their sensitivity to capillary anisotropy. A preliminary study indicates that λ^* and λ_T^* strongly depend on the alloy concentration. Thus, the dispersion in Fig. 8 may also reflect slight variations of the alloy concentration from one sample to the other. As shown by Fig. 6, the results are not G dependent, in the range of G/V explored. We have already discussed the role of sample thickness in Ref. [5]. This parameter is indeed crucial in one respect. A very small thickness blocks, to a certain extent, the transverse modes of instability that lead to the creation of new lamellae and could kill the tilted states. However, the dynamics of the tilt domains as such does not appear sensitive to sample thickness, in the 15–50-μm range [2].

C. Instability of the dynamically selected basic state

The wavelength-selection problem in lamellar eutectics may be phrased as follows: does a mechanism exist that tends to bring the system into a basic state of well-defined (but V-dependent) wavelength? Experimentally, the "selected" wavelength of lamellar eutectic patterns is close to the theoretical minimum-undercooling wavelength λ_m, which, in the range of G/V that we use, varies as $V^{-1/2}$ [6–10,22]. As just shown, the dynamically selected basic-state wavelength λ^* does not follow the $V^{-1/2}$ law. We can conclude from this fact alone that the dynamical wavelength selection by tilt domains cannot by itself provide the answer to the wavelength selection problem. This important conclusion needs, however, to be more carefully established.

It is generally believed, for empirical as well as theoretical reasons, that λ_m is, in fact, the lower stability limit of the basic state [6–10]. It is certain that the phase diffusion coefficient is not exactly zero at $\lambda=\lambda_m$ [23]. However, we have recently confirmed, in the CBr_4-C_2Cl_6 system and for $\eta\cong 0.5$, that λ_m is close to the threshold for the lamellar-extinction or pinching-off instability. We have measured, on the one hand, the threshold λ_{pinch} for this instability, and on the other hand the material parameters, the knowledge of which is necessary to calculate λ_m, in the Jackson-Hunt approximation: to experimental uncertainty, $(\lambda_{\text{pinch}})^2 V\cong\lambda_m^2 V=190\pm 30$ $\mu\text{m}^3\,\text{s}^{-1}$ [22]. The estimated $\lambda_m(V)$ curve is drawn in Figs. 7 and 8. For $V=1.54$ and 2.26 $\mu\text{m}\,\text{s}^{-1}$, λ^* is clearly smaller than λ_m. For $V=0.85$ and 1.22 $\mu\text{m}\,\text{s}^{-1}$, the difference between λ_m and λ^* is not larger than the experimental uncertainty. The numerical fit on the value of λ^*, in Fig. 8, indicates that $\lambda^*(V)$ crosses the $\lambda_m(V)$ curve at a velocity V_{cr} located between 0.85 and 1.22 $\mu\text{m}\,\text{s}^{-1}$. For $V=1.54$ and 2.26 $\mu\text{m}\,\text{s}^{-1}$, one thus expects lamellar extinctions to occur behind tilt domains. This we indeed observed, as pointed out above (see Fig. 4). On the other hand, for $V=0.85$ and 1.22 $\mu\text{m}\,\text{s}^{-1}$, we observed no lamellar extinction [see Fig. 5(b)]. At these velocities, the dynamically selected basic state is remarkably homogeneous (the lamellar-spacing dispersion is not larger than about 5%, i.e., hardly larger than the instrumental uncertainty) and appears stationary (the longest time for which this stationary could be checked was of the order of 500 s).

We have analyzed in more detail the lamellar-extinction process behind the domains at 1.54 and 2.26 $\mu\text{m}\,\text{s}^{-1}$. Figure 9 shows that these lamellar extinctions occur in a very regular way. The time elapsed between the emergence of a lamella from the trailing wall and its pinching off can be measured [that it is a well-defined quantity, at least at 1.54 $\mu\text{m}\,\text{s}^{-1}$, is proven by the fact that the row formed by the traces of the lamellar-extinction events in Fig. 9(a) is parallel to the trajectory of the trailing wall]. It is about 80 s at 1.54 $\mu\text{m}\,\text{s}^{-1}$, but only a few seconds at 2.26 $\mu\text{m}\,\text{s}^{-1}$. At 1.22 $\mu\text{m}\,\text{s}^{-1}$, it is at least 500 s. If we interpret this time as the transient duration for a lamellar-extinction instability to develop in a basic state of wavelength λ^*, this indirectly confirms that the difference between λ^* and $\lambda_{\text{pinch}}\cong\lambda_m$ rapidly de-

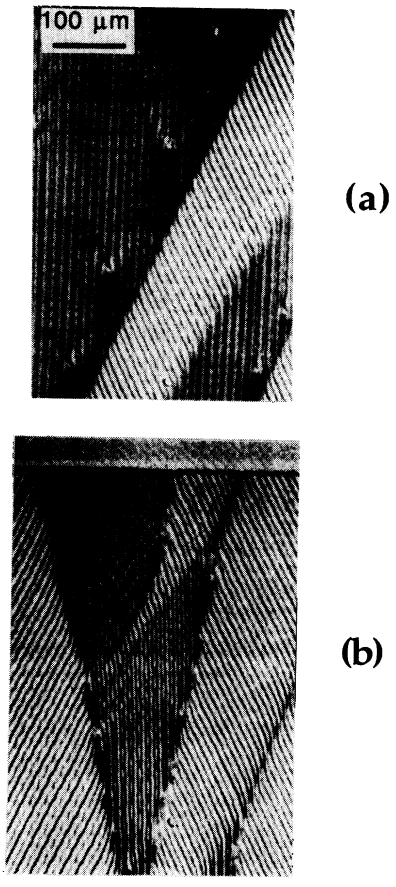

FIG. 9. Regular occurrence of lamellar deaths in the rear of tilt domains. (a) $V=1.54$ $\mu\text{m}\,\text{s}^{-1}$. Region near the border of the sample (on the left); (b) $V=2.26$ $\mu\text{m}\,\text{s}^{-1}$ (same magnification). The region between the tilt domains is oscillating. The oscillation triggers the nucleation of a new tilt domain. Note the solitary untilted wave in the rightmost tilt domain.

creases as V increases. On the other hand, it can be verified that the average proportion of lamellar pairs that disappears is approximately $(\lambda_m - \lambda^*)/\lambda_m$, confirming that, beyond the lamellar-extinction row, the basic state has almost completely relaxed to the wavelength λ_m.

These observations clearly establish that the dynamically selected basic state is unstable in a certain range of velocities. Dynamical wavelength selection by tilt domains is not, in general, a mechanism by which the system can stabilize at long times in a basic state of wavelength approximately λ_m. Incidentally, our observations also indirectly confirm that the threshold for the lamellar-extinction instability, λ_{pinch}, is a well-defined quantity, close to λ_m.

D. Solitary untilted waves, sources, and irregular regime

We have studied so far the dynamics of an isolated domain invading the basic state. We shall now consider the dynamics on the scale of a whole eutectic grain, when tilt domains are regularly emitted at the boundaries of the grain. At $V < V_{\text{cr}}$, the dynamically selected basic state is stable. Then, the permanent regime established at some distance from the boundaries is an alternation of tilt domains and basic-state regions in their dynamically selected state. Let us briefly describe what happens at $V > V_{\text{cr}}$, when the basic-state regions are unstable.

The initial stages of the process, which can be observed near the sites from which tilt domains are emitted, are illustrated by Fig. 10. Consider, in this figure, the basic-state region limited by the trailing wall of domain 3 (velocity v_{R3}) and the leading wall of domain 4 (velocity v_{A4}). A first stage consists in the rapid invasion of this region, as a consequence of the lamellar extinctions which occur in it. Because of these lamellar extinctions, the wavelength just ahead of the leading wall 4 is larger than the one just behind the trailing wall 3. Thus, v_{A4} is larger than v_{R3}. When the width of this region has become too small for lamellar extinctions to have time to occur, v_{A4} is still a little higher than v_{R3}, indicating that the rear wavelength λ_R is slightly larger than λ^*. In some cases, the two tilt domains finally merge into one larger domain and the basic-state region disappears altogether. In other cases, probably when the phase mismatch of the two tilted patterns is large, the width of the basic-state region stops when it reaches a very small value and then remains constant. In Fig. 10, this final configuration has already been reached by the 1-2 and 4-5 basic-state regions [see also Fig. 9(b)]. Another example is shown at a higher magnification in Fig. 11. Because its width is smaller than that of the domain walls, we believe that this stable configuration is a well-defined localized defect, a solitary "untilted" wave traveling in the tilted state. The phase jump of the tilted state on crossing this defect is 2π, within experimental uncertainty.

When the two boundaries of a grain are slanting and divergent, they both emit tilt domains in the grain. These domains moving in opposite directions meet near the center of the grain. Their meeting can give rise to two types of spatiotemporal structures. One of them is the

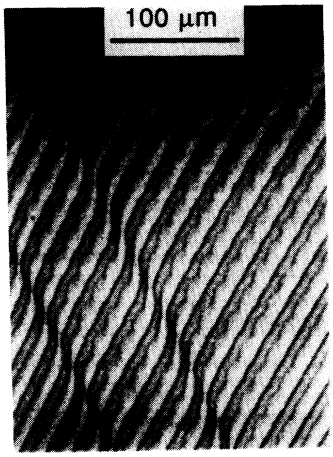

FIG. 11. "Solitary untilted wave" in the tilted state. An asymmetric, "optical" oscillation is also visible. This oscillation is frequently encountered, but is generally observed to vanish at long times.

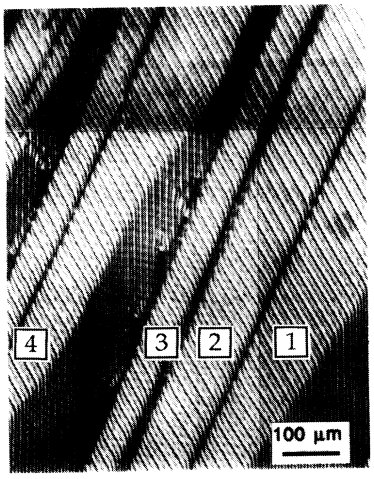

FIG. 10. Progressive disparition of basic-state domains and formation of localized defects. Lamellar extinctions can be seen in the rear of domain 3. Region near the border of the sample (on the left). $V = 1.54\ \mu\text{m s}^{-1}$.

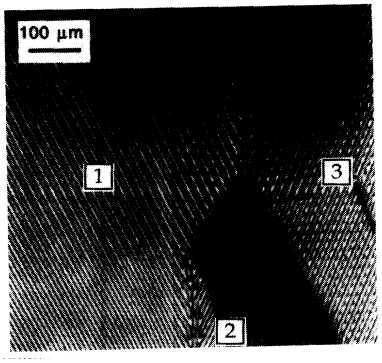

FIG. 12. "Source" created by tilt domains of opposite signs meeting in a quasi-isotropic grain. After its collision with domain 2, domain 1 keeps on moving to the right until it meets domain 3. $V = 2.26\ \mu\text{m s}^{-1}$.

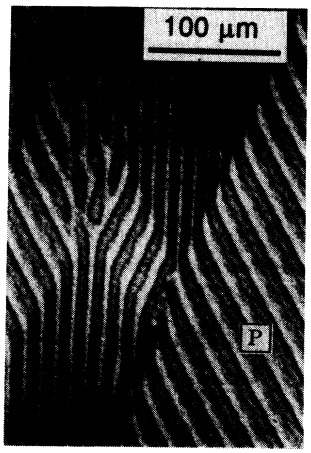

FIG. 13. Nucleation of a secondary tilt domain in the rear of a primary (P) one. $V=1.54\ \mu m\,s^{-1}$.

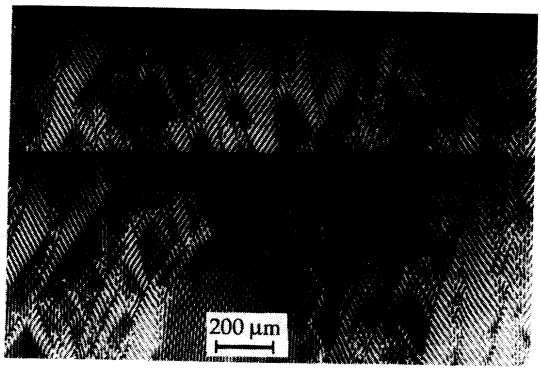

FIG. 14. Irregular regime generated by the nucleation of secondary domains. Oscillations at twice the basic wavelength are also present. $V=2.26\ \mu m\,s^{-1}$.

complex interplay of lamellar extinctions and lamellar creations described in Ref. [2] and visible, for instance, in Fig. 13. The other is the localized "source" emitting lamellae tilted alternatively to the right and to the left. Examples of such sources locked onto an underlying grain boundary have been given previously (see Fig. 4 of Ref. [6]). Figure 12 shows a source which bears no relation to a grain boundary (the source was somewhat irregular in the region shown, but stabilized at long times). This is demonstrated by the lateral displacement of the source, which is due to the unequal widths of the colliding domains and takes place within a given grain. Sources were observed only at $V=2.26\ \mu m\,s^{-1}$ and not in all grains (see below).

Solitary untilted waves and sources are localized defects, which does not alter the fact that the regime installed over the front is basically a homogeneous tilted state. A very different regime is observed in some eutectic grains, where the lamellar extinctions in the rear of a primary domain trigger the nucleation of secondary domains (Fig. 13). The occurrence of this nucleation is explained, basically, by the large increase of the local lamellar spacing following a lamellar extinction [2]. Once nucleated, the secondary domain travels through the rear basic-state region until it meets the next primary domain. Then the tilt domains are (partially) destroyed, i.e., the basic state is locally restored. A spatiotemporally disordered, apparently nondecaying regime results from this constant interplay between the tilt instability and the lamellar-extinction instability (Fig. 14). Whether this regime is intrinsic or driven by permanent emission of tilt domains at grain boundaries is for the moment unclear.

IV. CONCLUSION

The main results of this study are as follows.

(i) The dynamics of tilt domains in our experimental system is in complete agreement with theoretical predictions [4,17]. Tilt domains are regions of space-filling, stationary, tilted states of the system. The sweeping of the front by tilt domains is a wavelength selection mechanism—the dynamical wavelength selection by tilt domains—for both the tilted state within the domains and the basic state outside the domains.

(ii) In the range of pulling velocities that we have explored, the dynamically selected tilted-state wavelength is close to the homogeneous tilt bifurcation threshold. It varies as $V^{-1/2}$, within experimental uncertainty. The dynamically selected basic-state wavelength decreases much more rapidly than $V^{-1/2}$ as V increases. We have no explanation for this fact (which does not contradict the $\lambda\sim V^{-1/2}$ scaling law, since the latter should hold only for homogeneous states).

(iii) The dynamically selected basic-state wavelength is not the "selected" wavelength of lamellar eutectics, which is known to vary approximately as $V^{-1/2}$ in the range of velocities and thermal gradients in which our experiments are performed. Above a velocity V_{cr}, the dynamically selected basic state is unstable against the lamellar-extinction instability. The wavelength selection problem in lamellar eutectics remains an open one.

ACKNOWLEDGMENTS

The authors acknowledge many valuable discussions with B. Caroli, C. Caroli, and C. Misbah. They are grateful to B. Caroli and C. Caroli for their critical reading of the manuscript. They greatly thank R. Mellet (Centre National des Télécommunications, Bagneux, France) for providing them with zone-refined products. This research was supported by the Centre National d'Etudes Spatiales. J.M. is financially supported by the Société Péchiney.

[1] A. J. Simon, J. Bechhoefer, and A. Libchaber, Phys. Rev. Lett. **61**, 2574 (1988); J.-M. Flesselle, A.J. Simon, and A. Libchaber, Adv. Phys. **40**, 1 (1991).

[2] G. Faivre, S. de Cheveigné, G. Guthmann, and P. Kurowski, Europhys. Lett. **9**, 779 (1989).

[3] M. Rabaud, S. Michalland, and Y. Couder, Phys. Rev. Lett. **64**, 184 (1990).

[4] P. Coullet, R. E. Goldstein, and G. H. Gunaratne, Phys. Rev. Lett. **63**, 1954 (1989); R. E. Goldstein, G. H. Gunaratne, L. Gil, and P. Coullet, Phys. Rev. A **43**, 6700 (1991).

[5] G. Faivre and J. Mergy, Phys. Rev. A **45**, 7320 (1992).

[6] K. A. Jackson and J. D. Hunt, Trans. AIME **236**, 1129 (1966).

[7] J. S. Langer, Phys. Rev. Lett. **44**, 1023 (1980).

[8] W. Kurz and D. J. Fischer, *Fundamentals of Solidification* (Trans Tech, Aedermannsdorf, Switzerland, 1984).

[9] V. Seetharaman and R. Trivedi, Metall. Trans. **19A**, 295 (1988).

[10] B. Caroli, C. Caroli, G. Faivre, and J. Mergy, J. Cryst. Growth **118**, 135 (1992).

[11] K. Kassner and C. Misbah, Phys. Rev. Lett. **65**, 1458 (1990); **66**, 522 (1991).

[12] K. Kassner and C. Misbah, Phys. Rev. A **44**, 6533 (1991).

[13] K. Kassner and C. Misbah (unpublished).

[14] In the limit of small Péclet numbers ($\lambda/l \ll 1$, where $l=D/V$ is the diffusion length and D is the diffusion coefficient in the liquid), the properties of space-filling, homogeneous patterns depend on only two quantities, which can be taken as ld/λ^2 and l/l_{thermal}, where d is the capillary length and $l_{\text{thermal}} \sim V/G$ is the thermal length. When the latter variable is smaller than about 0.5, the dependence on it (i.e., on G/V) is negligible [12]. We have shown in [5] that our experiments are performed under these small-Péclet-number and small-G/V conditions.

[15] K. Brattkus, B. Caroli, C. Caroli, and B. Roulet, J. Phys. (Paris) **51**, 1847 (1990).

[16] The continuity of the lamellae through a wall separating two homogeneous states 1 and 2 implies that $(v-V_{x1})/\lambda_1 = (v-V_{x2})/\lambda_2$, where v is the velocity of the wall, λ_i is the wavelength, and V_{xi} is the drift velocity of state i. Knowing that, for tilt domains, $\lambda_T > \lambda_A, \lambda_B$ and $V_{xA}, V_{xB} \cong 0$, it is easily verified that $v_A - V_B$ has the same sign as $\lambda_A - \lambda_B$. In particular, $v_A = v_B$ is equivalent to $\lambda_A = \lambda_B$.

[17] B. Caroli, C. Caroli, and S. Fauve, J. Phys. I (Paris) **2**, 281 (1992).

[18] If the front shape can be approximated by the superposition of two Fourier components of wave numbers q and $2q$ and amplitudes $\rho e^{i\phi 1}$ and $\sigma e^{i\phi 2}$, the asymmetry parameter is $A = 2\phi_1 - \phi_2$. Such a situation is encountered, for example, in directional solidification of nematic liquid crystals slightly above the primary (i.e., planar to cellular) bifurcation of the system [1]. Then, coupled amplitude equations for ρ, σ, and A can be derived from the standard directional-solidification model [see W.-J. Rappel and H. Riecke, Phys. Rev. A **45**, 846 (1992) and earlier references therein] and the mechanism underlying the tilt bifurcation (called bifurcation to traveling-wave states by Rappel and Riecke) is identified as a resonant interaction between the modes q and $2q$. In eutectics, because the "solid" is two phased, no primary bifurcation exists. Even at a low pulling velocity, the stationary front has a complicated cellular shape, represented by a slowly converging Fourier series [6]. Therefore, the q-$2q$ analysis is not relevant to eutectics. The question of the equivalence, from the phenomenological viewpoint, between the model represented by Eqs. (1) and the q-$2q$ model is beyond the scope of the present paper.

[19] The full second-order expansion in powers of A and Φ consistent with the symmetry properties of our system contains six additional terms, which do not appear in Eqs. (1) [S. Fauve, S. Douady, and O. Thual, Phys. Rev. Lett. **66**, 385 (1990) and J. Phys. II (Paris) **1**, 311 (1991)]. As discussed in [17], these terms would not alter the tilt domains dynamics predicted by Eqs. (1) *qualitatively*. They are therefore irrelevant to our present purpose, which is *not* to fit quantitatively any model to the experimental measurements.

[20] There is a loose correlation between the stationary value of $|\phi_0|$ in the grain and the amplitude of the differences between the characteristics of opposite tilt domains. The data in Figs. 6 and 8 have been measured on tilt domains of a given sign in grains where $|\phi_0| \cong 0$.

[21] G. Faivre, C. Guthmann, and J. Mergy, in *Nonlinear Phenomena in Materials Science*, edited by G. Martin and L. Kubin (Trans. Tech. Aedermannsdorf, Switzerland, 1992), Vol. II, p. 1.

[22] J. Mergy, thèse, Université Paris 7 (1991). The basic state has been studied numerically, without approximation, by K. Kassner and C. Misbah, Phys. Rev. A **44**, 6513 (1991). In the range of G, V, η, and λ that we use, it is clear that the error on the value of λ_m arising from the use of the Jackson-Hunt approximation is much smaller than that due to the experimental uncertainties on the material parameters.

[23] B. Caroli, C. Caroli, and B. Roulet, J. Phys. (Paris) **51**, 1867 (1990).

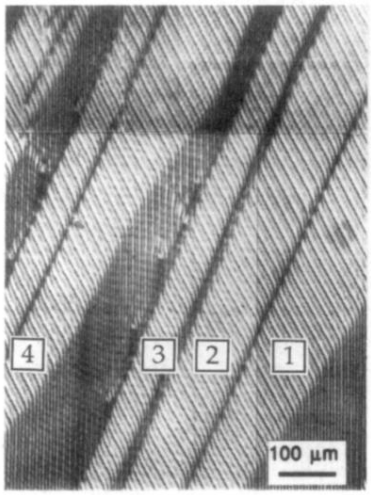

FIG. 10. Progressive disparition of basic-state domains and formation of localized defects. Lamellar extinctions can be seen in the rear of domain 3. Region near the border of the sample (on the left). $V = 1.54\ \mu m\ s^{-1}$.

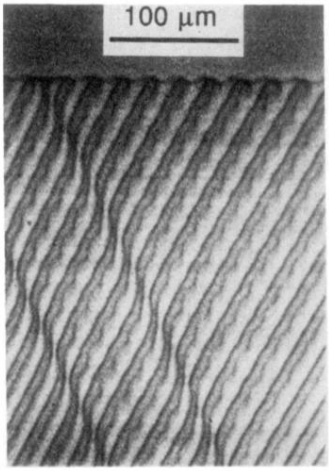

FIG. 11. "Solitary untilted wave" in the tilted state. An asymmetric, "optical" oscillation is also visible. This oscillation is frequently encountered, but is generally observed to vanish at long times.

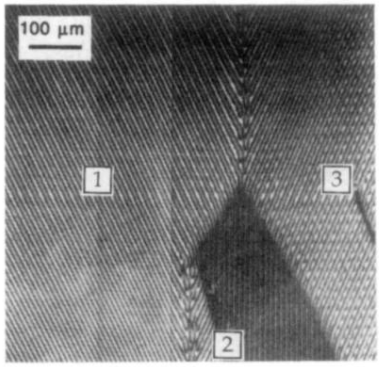

FIG. 12. "Source" created by tilt domains of opposite signs meeting in a quasi-isotropic grain. After its collision with domain 2, domain 1 keeps on moving to the right until it meets domain 3. $V = 2.26\,\mu\mathrm{m\,s^{-1}}$.

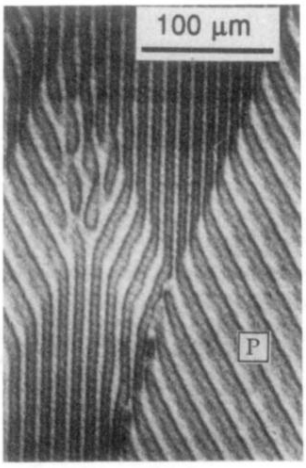

FIG. 13. Nucleation of a secondary tilt domain in the rear of a primary (P) one. $V = 1.54\ \mu m\, s^{-1}$.

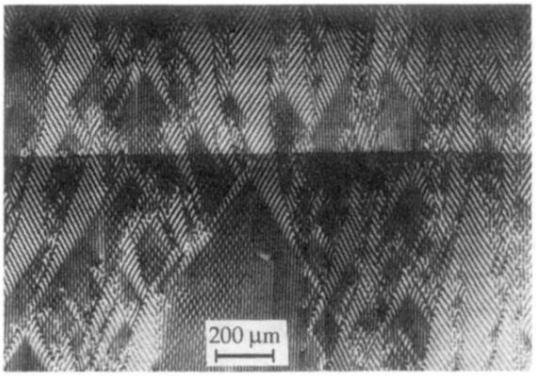

FIG. 14. Irregular regime generated by the nucleation of secondary domains. Oscillations at twice the basic wavelength are also present. $V = 2.26\ \mu\mathrm{m\,s^{-1}}$.

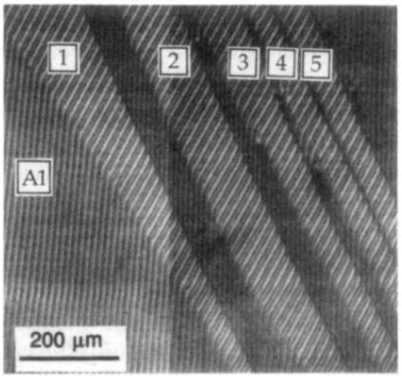

FIG. 4. Tilt domains emitted at the onset of the experiment described in Table I. $V = 1.54\ \mu m\, s^{-1}$. Photograph of the solid (the solidification front is out of the image). Time is running upwards. The domains are primary ones. Note the decrease of the basic-state tilt angle when the wavelength decreases. The white dots in the upper half of the photograph are traces left by lamellar extinctions (see text).

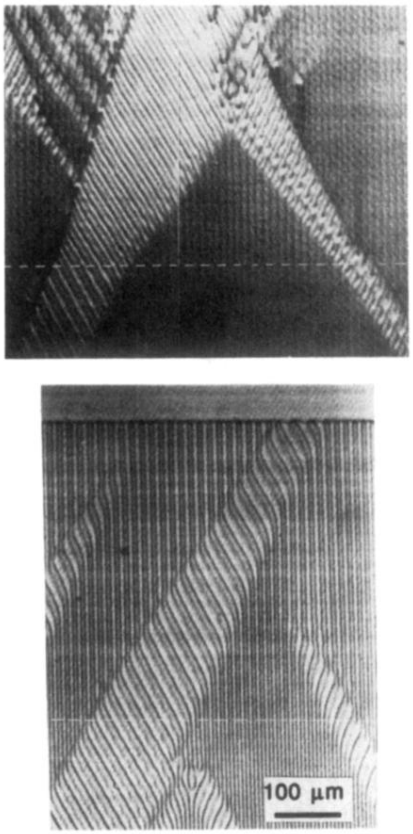

FIG. 5. Effect of velocity jumps on preexisting tilt domains. (a) Jump from 1.54 to 2.26 $\mu m\,s^{-1}$; (b) jump from 1.22 to 0.85 $\mu m\,s^{-1}$. Broken lines, velocity jump.

FIG. 9. Regular occurrence of lamellar deaths in the rear of tilt domains. (a) $V = 1.54\ \mu m\,s^{-1}$. Region near the border of the sample (on the left); (b) $V = 2.26\ \mu m\,s^{-1}$ (same magnification). The region between the tilt domains is oscillating. The oscillation triggers the nucleation of a new tilt domain. Note the solitary untilted wave in the rightmost tilt domain.